

Article

Spectroscopic Analysis of CF_4/O_2 Plasma Mixed with N_2 for Si_3N_4 Dry Etching

Wan Soo Song, Ju Eun Kang and Sang Jeon Hong * 

Department of Electronics Engineering, Myongji University, Myongji-ro 116, Yongin-si 17058, Korea; wansoo2603@mju.ac.kr (W.S.S.); ysy06024@mju.ac.kr (J.E.K.)

* Correspondence: samhong@mju.ac.kr; Tel.: +82-31-330-6374

Abstract: Silicon nitride (Si_3N_4) etching using CF_4/O_2 mixed with N_2 has become very popular in 3D NAND flash structures. However, studies on Si_3N_4 dry etching based on optical emission spectroscopy (OES) are lacking; in particular, no study has reported the use of OES for analyzing N_2 -mixed CF_4/O_2 plasma. Thus, this study demonstrates an OES-based approach for analyzing a mixed-gas plasma for etching Si_3N_4 thin films. The state of each single gas plasma of CF_4 , O_2 , and N_2 as well as that of mixed plasmas of heterogeneous gases CF_4/O_2 , CF_4/N_2 , and O_2/N_2 was investigated to analyze the mixed-gas plasma. Furthermore, the amount of N_2 in the CF_4/O_2 plasma varied from 0 to 8 sccm. The relationship between the OES analysis results and the Si_3N_4 etch rate was subsequently established using Si_3N_4 film etching, and the explanation was verified through a chemical reaction modeling and surface reaction. Therefore, our study confirmed the alteration in chemical species and quantity that occurred when N_2 was added to CF_4/O_2 plasma and the effect of the alteration on Si_3N_4 etch.

Keywords: silicon nitride; optical emission spectroscopy; etch; mixed-gas plasma; actinometry



Citation: Song, W.S.; Kang, J.E.; Hong, S.J. Spectroscopic Analysis of CF_4/O_2 Plasma Mixed with N_2 for Si_3N_4 Dry Etching. *Coatings* **2022**, *12*, 1064. <https://doi.org/10.3390/coatings12081064>

Academic Editors: Qi Hua Fan and Jang-Hsing Hsieh

Received: 9 June 2022

Accepted: 26 July 2022

Published: 27 July 2022

Publisher's Note: MDPI stays neutral with regard to jurisdictional claims in published maps and institutional affiliations.



Copyright: © 2022 by the authors. Licensee MDPI, Basel, Switzerland. This article is an open access article distributed under the terms and conditions of the Creative Commons Attribution (CC BY) license (<https://creativecommons.org/licenses/by/4.0/>).

1. Introduction

Si_3N_4 has been extensively used as a chemical diffusion barrier against water molecules and Na. Furthermore, it acts as a good insulator with high thermal stability and has been used in the fabrication of microelectronic and semiconductor devices. Si_3N_4 thin films are used in various semiconductor processes as an etch stop layer and as a hard mask for etching as well as for passivation and other functions. Si_3N_4 deposition technologies and applications in semiconductor fabrication have already been comprehensively described [1]. Despite its various applications, the precise control of Si_3N_4 -related processes is irrelevant compared with other dielectrics such as SiO_2 , low-*k*, and high-*k* materials. The processes related to dielectric films have been investigated in terms of film properties, process uniformity, and plasma [2–6]. Because Si_3N_4 has been used as a charge trap layer in case of NAND memories, the application of Si_3N_4 films in 3D NAND flash memory fabrication has increased [7,8]. The anticipated etch challenges for the 3D NAND flash technology were considered with the increasing number of 3D NAND oxide/nitride (ON) gate stacks [9].

Si_3N_4 etching was first investigated using CF_4 and O_2 gas combinations to produce patterns in microcircuits [10,11]. The high etch rate in the hard mask strip process was studied in the 2000s using $\text{SF}_6/\text{O}_2/\text{N}_2$ gas chemistry [12]; however, NF_3 replaced SF_6 in the early 2010s because SF_6 was listed as having a high global warming potential [13,14]. With the development of 3D NAND flash memory, various gas mixtures, such as $\text{NF}_3/\text{O}_2/\text{N}_2/\text{He}$, CHF_3/O_2 , CF_4/H_2 , and CF_4/D_2 , have been used to satisfy the required etch profiles [15–19]. Si_3N_4 has traditionally been used as a selective etch mask over silicon dioxide because of its hardness and chemical resistance to fluorinated gas species. However, the dry etching of ON gate stacks in 3D NAND requires that the high aspect ratio ON dielectric gate stacks be simultaneously completed in the same process chamber; the recipe control for this

process thus becomes more challenging compared with any other conventional dry etching process. The in situ monitoring of ON gate stack deposition was proposed as a basis to ease the concerns of etching the multiple pairs of the two dielectric materials in the same plasma etch chamber [20]. The use of plasma process monitoring is recommended to better understand the changes occurring inside the plasma etching chamber and realize successful dielectric etching such as etch depth, profile, etc. with the plasma information which can be deduced/calculated through the plasma monitoring in 3D NAND. A frequently used plasma monitoring method is optical emission spectroscopy (OES). Research on plasma during the SiO₂ etching process has been actively conducted, but research on plasma during Si₃N₄ gate stack etching is limited because of the complications of nitrogen-related radical species in the plasma. The results of silicon dioxide OES data analysis and etch rate virtual metrology have been analyzed, and they are satisfactory in the field of plasma etching [2,21]. Recently, an OES study predicted the properties of a Si₃N₄ layer for solar cell applications [22]; however, this study is limited specifically to the surface chemistry and deposition rate. Electron temperature and density have been theoretically estimated using multiple population/depopulation models [23–25]. Although electron temperature and density are important criteria in understanding plasma physics, spontaneously determining the plasma state in mixed-gas plasma is difficult.

Artificial intelligence or machine learning modeling is suggested to examine the plasma properties in the gas plasma mixture; however, they still lack the physical interpretation to understand the behavior of gaseous species in the plasma. Chien et al. demonstrated virtual metrology modeling with statistics-based and dynamics-inspired OES data [26]; however, it is important to understand the plasma chemistry and qualitative/quantitative number of reactive species to further comprehend the underlying phenomena in the plasma during Si₃N₄ etching. Kim et al. demonstrated an example of how to use OES for spectroscopic analysis [27]. They discovered the cause of the difference in etch rates between NF₃/Ar and F₃NO/Ar plasma using OES data. However, a spectroscopic analysis study on CF₄/O₂ plasma mixed with N₂ for Si₃N₄ dry etching is still insufficient.

Real-time and non-invasive process diagnosis technology is currently the research focus to improve yield. Therefore, processing the diagnosis of Si₃N₄ dry etch for ON stack that has not been previously studied using OES is important; this is easy to use and install. Additionally, comparing the number of reactive species in the plasma mixed with three gas species is necessary, which rarely existed before, to correlate the reason and relationship with the process result. Consequently, this study proposes a method for applying OES in the mixed-gas plasma, particularly CF₄/O₂ mixed with N₂ under Si₃N₄ dry etching conditions, to support the plasma monitoring capabilities of OES regarding plasma process diagnostics. OES data were obtained for each plasma of CF₄, O₂, and N₂ to define generated radicals and ions in each wavelength. Similarly, OES data from CF₄/O₂, CF₄/N₂, and O₂/N₂ plasma were obtained. Finally, we investigated the effects of adding N₂ to CF₄/O₂ plasma. Therefore, the best peak in CF₄/O₂ mixed with N₂ plasma was discovered. Thus, when the N₂ flow rate was increased, the amount of F radical decreased and nitrogen reacted with radicals such as CN and NO. Furthermore, by etching under the same experimental conditions as CF₄/O₂/N₂ plasma, it was verified that F radicals have a similar relationship with the Si₃N₄ etch rate. The chemical simulation and surface reaction explained the reason for the F radicals trend and etch rate.

2. Experiment

Plasma was generated using an inductively coupled plasma (ICP)-type dry etcher, developed by Plasmart Inc. (Daejeon, Korea). Figure 1 shows that the equipment comprises a 13.56 MHz ICP source and a 12.56 MHz bias power, which was not used in this experiment, with separated RF matching units. The chamber has a diameter of ~315 mm and a 6-inch metal chuck in the center. The vacuum system comprises an oil rotary pump, the base pressure of which can reach 10 mTorr, and a turbo molecular pump that holds the pressure

below a few tens of mTorr during the gas injected vacuum condition. Process gases through the mass flow controllers are combined before injecting them in the showerhead located at the top of the chamber, and the process steps are controlled using programmable logic controllers. There are two sidewall viewports in the etch system. The front side viewport was used for operational visual inspection, whereas the side viewport was used to collect the OES data from the plasma glow discharge during the experiment. The spectrometer used is the SM245, by Korea Spectral Products (Seoul, Korea), which has a spectral range of 200–1050 nm and an optical resolution of ranges of <10 nm full width at half maximum. A Si_3N_4 thin film deposited via low-pressure chemical vapor deposition (LPCVD) on a 4-inch wafer was used in the etching process. In the experiment, the wafer was sliced and used as a coupon. A reflectometer (ST2000–DLS, KMAC Co., Daejeon, Korea) was used to measure the thickness of Si_3N_4 before and after etching.

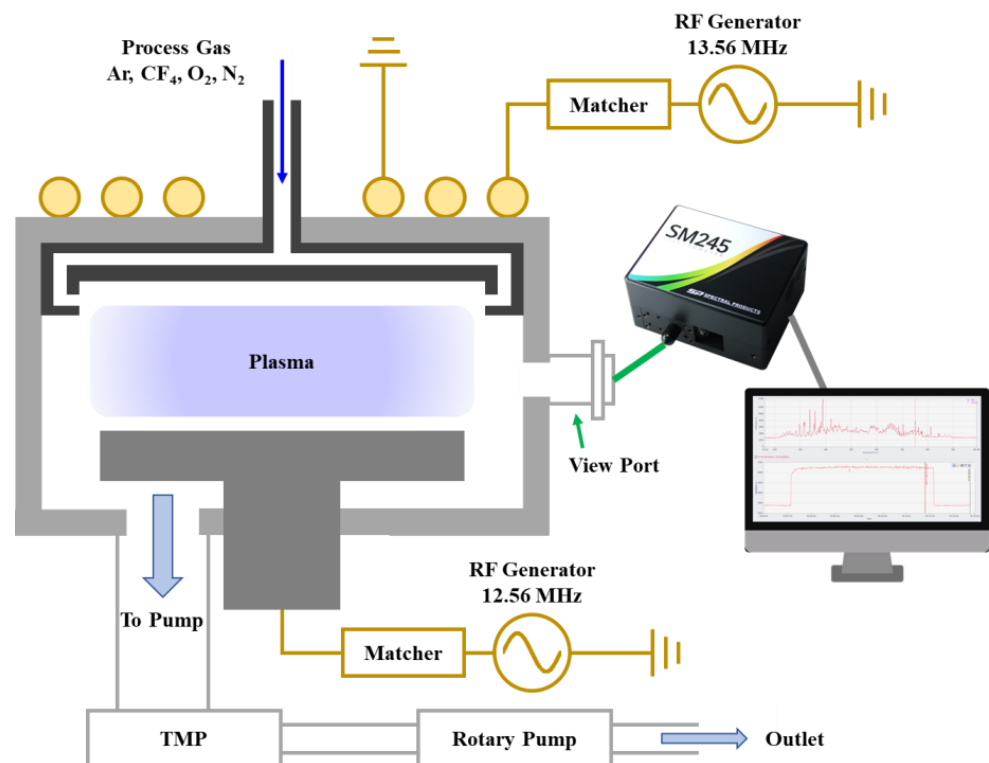


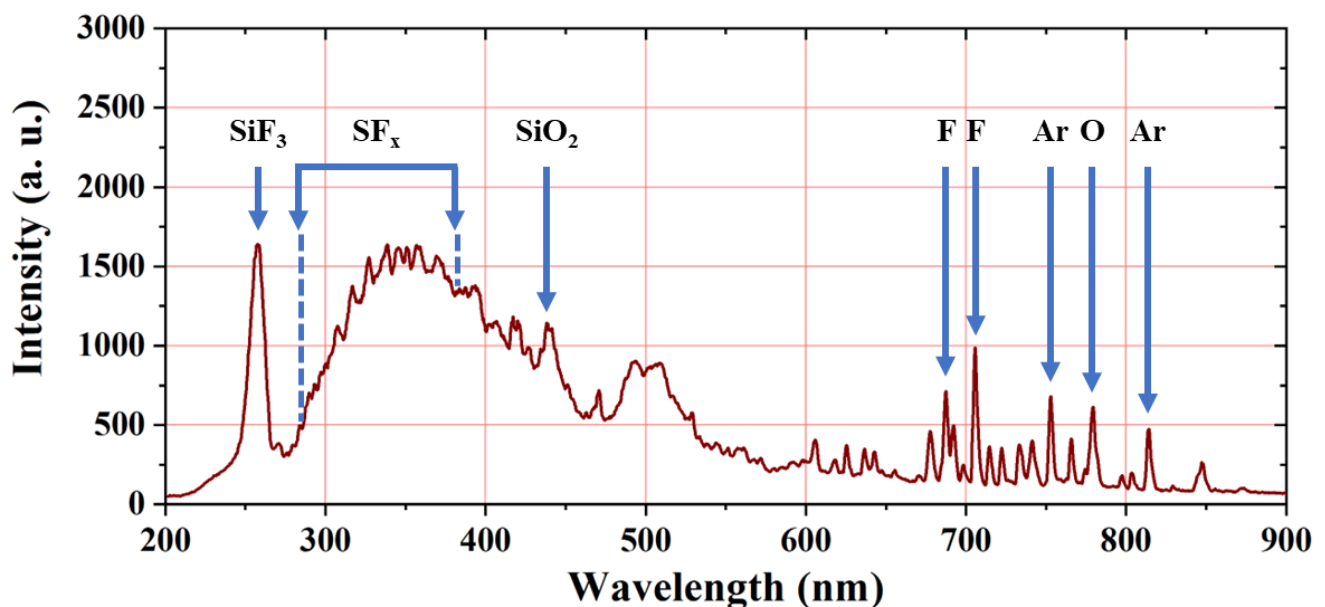
Figure 1. Schematic of the ICP-type chamber with an RF power, vacuum, and sensing units.

Table 1 shows the process recipes. RF source power, pressure, and temperature were set to 300 W, 5 mTorr, and room temperature, respectively, in a cleanroom environment. Two key processes comprise the following procedure: a preliminary process to acquire and analyze the OES data and the main process for etching Si_3N_4 . In the preliminary process, only the 6-inch dummy wafer was placed on the chuck, and the process was conducted. In contrast, the coupon wafer was located on the 6-inch dummy wafer in the main process, and the experiment was performed. The plasma emission spectra of each form of gas, CF_4 , O_2 , or N_2 , with flow rates of 40 sccm, were sequentially introduced to the chamber to generate the plasma as a basis for the OES investigation during the Si_3N_4 etch process. Then, a 20-sccm gas flow of the individual gas out of two mixed gases was investigated to understand the interaction of two gas species in terms of atomic/molecular spectroscopy. Finally, $\text{CF}_4/\text{O}_2/\text{N}_2$ were injected 40/4/0 ~8 sccm. Additionally, 4 sccm Ar was injected for all cases to examine the radical ratios at a wavelength of 750.4 nm [28]. In the main process, Si_3N_4 films were etched under the same $\text{CF}_4/\text{O}_2/\text{N}_2$ conditions.

Table 1. Process recipe of all single and mixed gas plasmas.

No.	RF Power [W]	Pressure [mTorr]	Gas [sccm]			
			CF ₄	O ₂	N ₂	Ar
1			40	0	0	
2			0	40	0	
3			0	0	40	
4			20	20	0	
5			20	0	20	
6	300	5	0	20	20	4
7			40	4	0	
8			40	4	2	
9			40	4	4	
10			40	4	6	
11			40	4	8	

The OES collects plasma glow discharge light and presents it as a spectrum. Atoms, molecules, and ions can be observed in the mixed-gas plasma shown in Figure 2; however, the identification of the correct gas-phase species is challenging because of the complex glow discharge light emission mechanism of ionization, excitation, vibration, and rotation or wavelength shifting of the spectrometer. The chemical species should be specified to determine the precise chemical species represented by the wavelength. Thus, OES data for a single gas plasma must be obtained first. Then, CF₄/O₂, CF₄/N₂, and O₂/N₂ plasma data should be obtained to confirm the wavelength of heterogeneous compounds, such as CO, CN, and NO. Our main objective is to discover three-no or small three-element compounds in CF₄/O₂/N₂ plasma, but we must examine the wavelengths of the compounds and identify the chemical species represented by each wavelength. Table 2 summarizes the information about the wavelength used in the Results and Discussion section.

**Figure 2.** An example of OES data of atoms and molecules in SF₆/O₂/Ar plasma.

Chemkin-Pro was used to study the chemical species and reactions within the plasma to explain the findings of the main process. CF₄, O₂, and N₂ were introduced into a modeled tubular reactor, which had a similar size to the chamber in use. The same RF power, pressure, and flow rates of CF₄, O₂, and N₂ were employed as that in No. 7–11 in Table 1.

Table 2. Information on wavelengths used in the Results and Discussion section with their original wavelength.

Species	Wavelength (nm)	Shifted Wavelength (nm)
Ar	750.4	750.87
F	712.8	713.1
	703.7	704.1
	685.6	686.5
O	844.6	845.08
	777.1	778.01
NO	259.2	259.07
	247.9	247.42
N ₂	394.3	394.79
	380.56	381.1
	337.1	337.62
CN	388.43	388.92
CO	483.5	483.61
	438	438.16
	297.7	297.73
	283	283.27

3. Results and Discussion

In the experiment preparation step, we performed a dry run as an equipment and system check for the experiment to avoid any unexpected experimental situations, including a dry etch chamber and OES data collection. We discovered an unexpectedly high number of photon counts associated with CN peaks below 400 nm in the spectrum while collecting OES data. The observation of CN peaks in CF₄ plasma is unusual because no external N₂ is supplied to the chamber. We hypothesized that the chamber's air leak caused nitrogen to have CN-related peaks, and hence the chamber's O-ring was replaced before initiating the actual experimental process. Figure 3 shows the OES signal before and after replacing the chamber's O-ring. Figure 3a shows that the CN peak intensity was substantially higher than that of the CF_x peak. Figure 3b shows that the CN peak was significantly reduced after the O-ring was replaced. Unfortunately, the OES data still indicated that there was some amount of nitrogen in the chamber, and the subsequent experimental results considered an acceptably small amount of air leak in the etch system.

Figure 4 shows CF₄, O₂, and N₂ single-gas plasma. In the case of CF₄, the CF_x band was observed at wavelengths of 240–400 nm. The fluorine (F) band was detected at 704.1 nm instead of 703 nm, which is recommended in the NIST mass spectral library, possibly owing to a measurement error attributed to the spectrometer calibration. An oxygen atom band (O) at 778 and 845 nm, the N₂ first positive system (FPS), N₂⁺ first negative system (FNS), and N₂ second positive system (SPS) were observed in the case of O₂ and N₂ single-gas plasmas.

Figure 5 shows the emission spectra of mixed-gas plasmas: CF₄/O₂, CF₄/N₂, and O₂/N₂. Although the CF₄/O₂ plasma contains multiple radicals such as C, C₂, COF, and CF_x, the CO band at ~250–600 nm, F bands at 704.1 and 713.1 nm and oxygen bands at 778 and 845.1 nm were the most prominent. The N₂ FPS, N₂ SPS, CN violet, and C₂ swan bands were observed in the case of CF₄/N₂ plasma. The O₂/N₂ plasma shows species similar to those observed in the single-gas O₂ and N₂ plasmas, including NO bands in the range of 210–290 nm.

Finally, Figure 6 shows the NO, N₂, and CO bands with numerous atom species in the case of CF₄/O₂/N₂ plasma. The deviation in the measured wavelengths of approximately ±1 nm from the previously reported values is attributed to the inherent calibration error of the spectrometer.

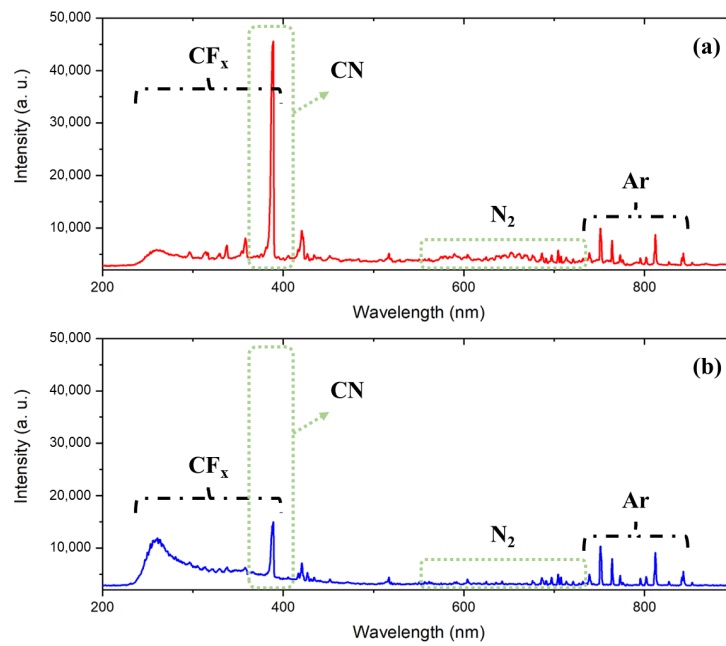


Figure 3. Leakage reduction verification using CF₄ plasma. (a) before and (b) after O-ring replacements. After replacement, the intensity of CN and N₂ drastically reduced. However, the remaining CN and N₂ peaks were observed, suggesting that the leakage was not completely controlled.

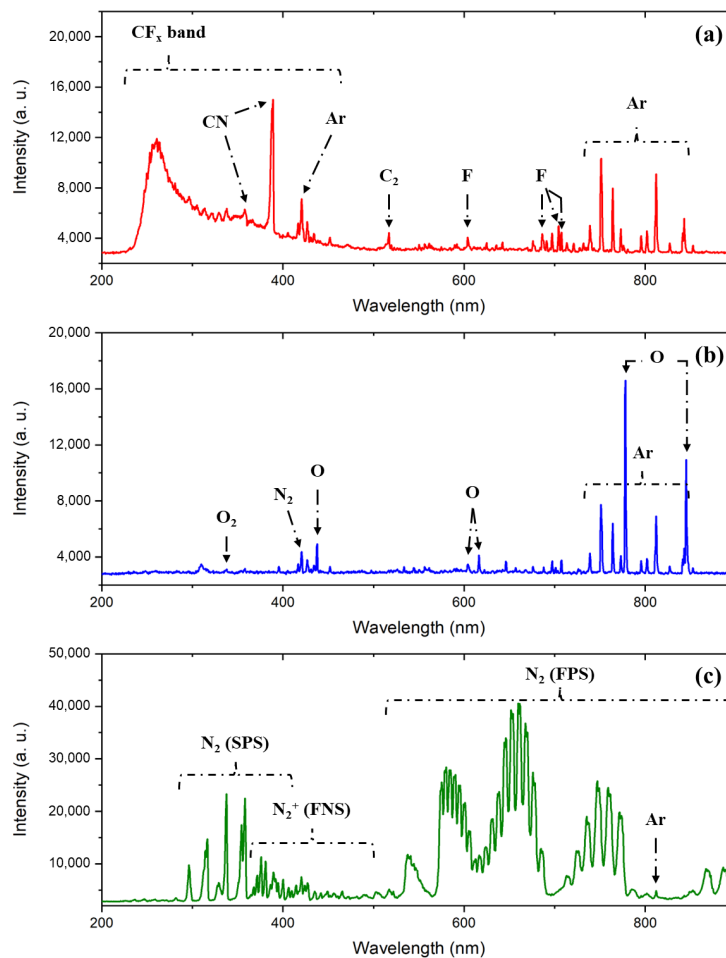


Figure 4. (a) CF₄, (b) O₂, and (c) N₂ OES spectrum. N₂-related peaks in (a) and (b) appeared due to air leakage.

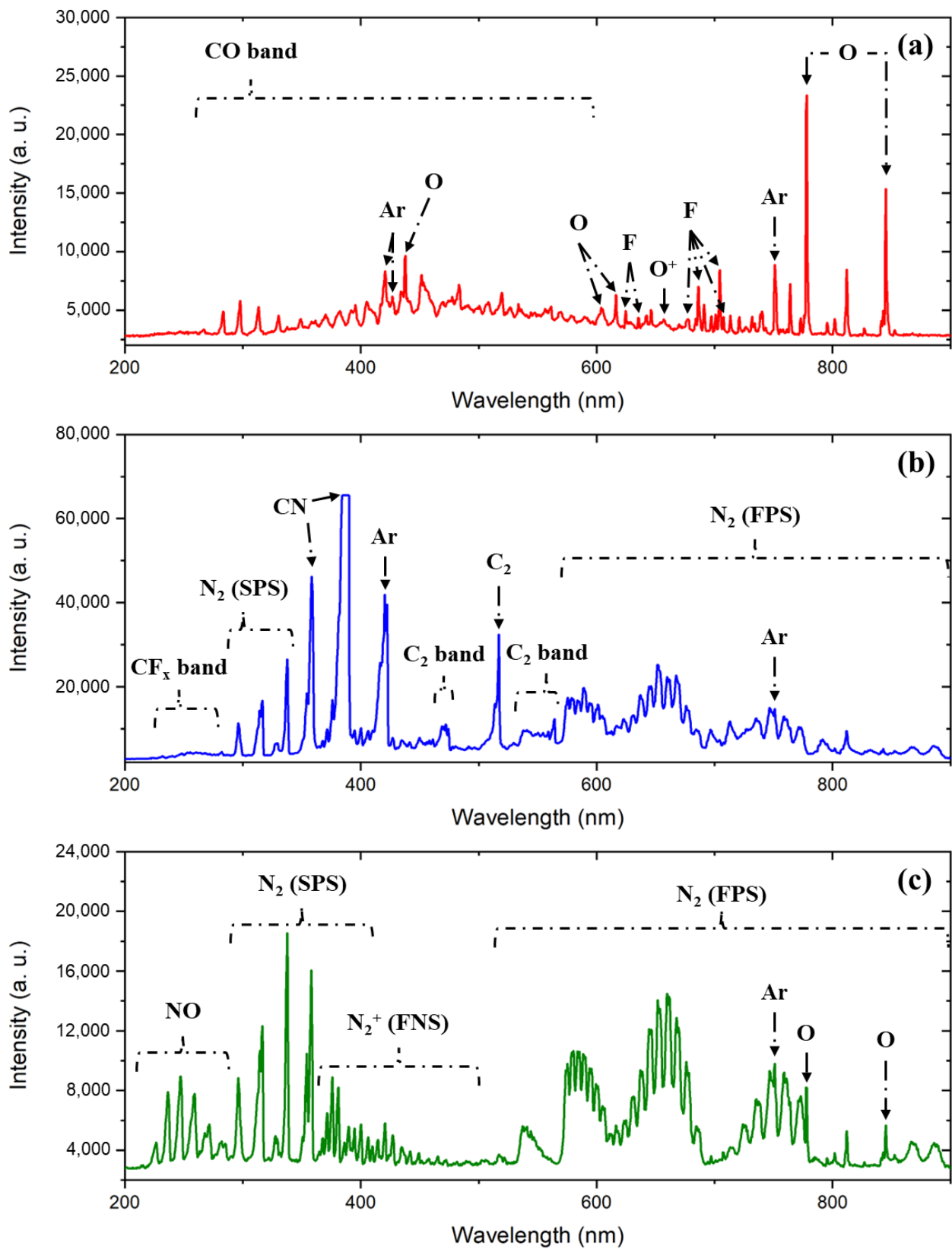


Figure 5. (a) CF_4/O_2 , (b) CF_4/N_2 , (c) O_2/N_2 OES spectrum. Molecular species such as CO, CN, and NO, generated by the reactions of two injected gas species, are observed.

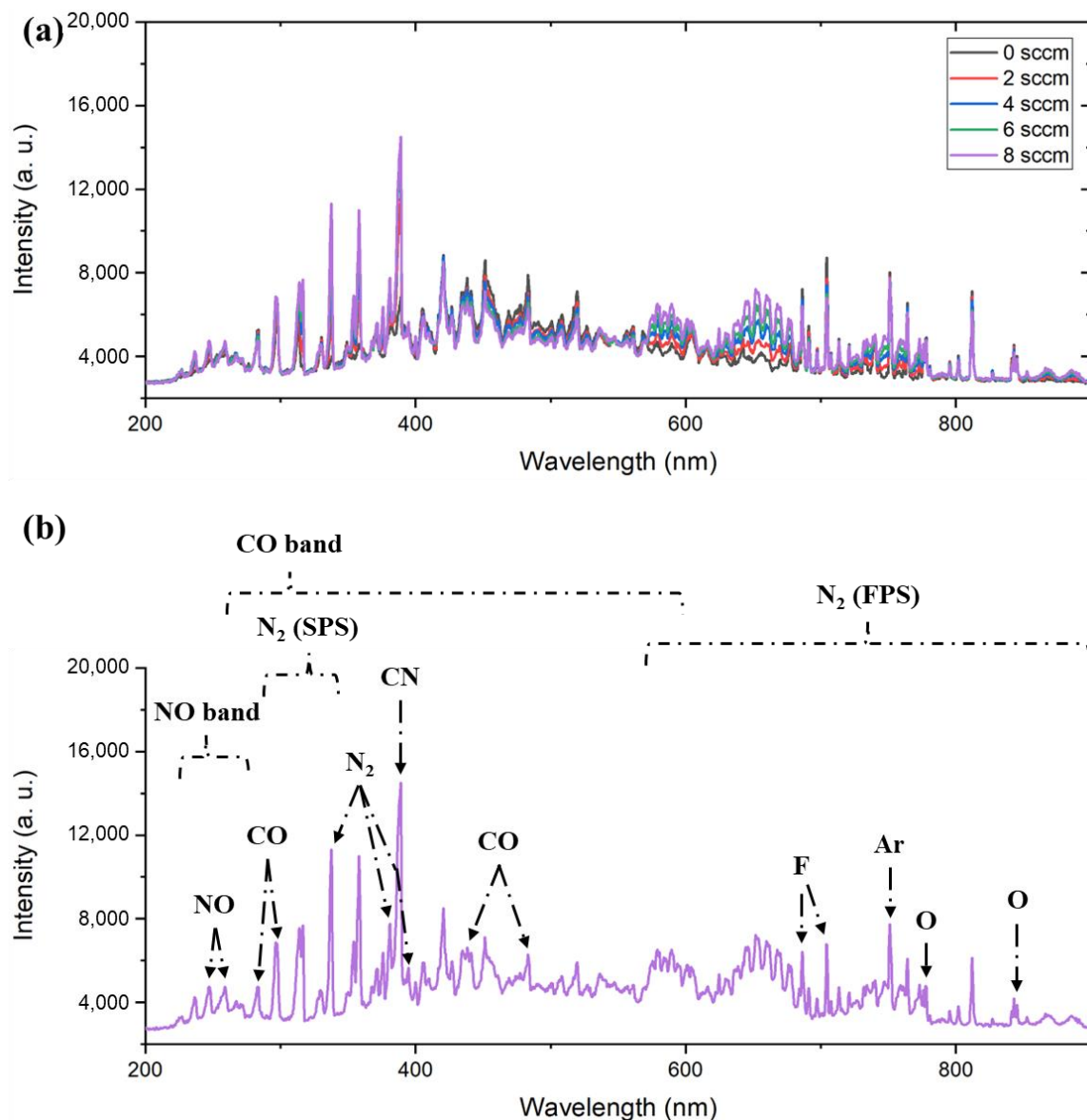


Figure 6. The spectrum of CF₄/O₂/N₂ plasma (a) according to N₂ flow rate and (b) selected wavelength of each species in the N₂ and 8-sccm cases. We selected the wavelengths of atoms and molecules. Representative peaks were used in the case of molecules as the OES spectrum of molecules has band-shaped emission spectra.

The Ar actinometry method was used to analyze the chemical species. The relationship of the emission light intensity of species X at a typical wavelength, λ , is expressed as follows:

$$I_X = C_X(\lambda) N_X n_e \int_{\epsilon_X}^{\infty} \sigma_X(\epsilon) f(\epsilon) \sqrt{\frac{2\epsilon}{m_e}} d\epsilon, \quad (1)$$

where $C_X(\lambda)$ is a quantity that depends on the response of the spectrometer and light collection system at wavelength, λ , N_X is the density of species X in the ground state, n_e is the electron density, $\sigma_X(\epsilon)$ is the electron excitation cross section, ϵ_X is the threshold energy for the considered process, $f(\epsilon)$ is the electron energy distribution function, and m_e is the mass of the electron. The choice of wavelength is crucial when applying the Ar actinometry method. Only electron impact excitation should influence the emission wavelength, and the cross section of excitation type A used as an actinometer and type X selected for analysis

should follow a similar pattern [29]. Then, it can be represented as follows by dividing both intensities using Equation (1):

$$\frac{N_X}{N_A} \propto \frac{I_X}{I_A}, \quad (2)$$

where N_A and I_A are the density and measured intensity of the actinometer, respectively. In this research, Ar at 750.87 nm was used as an actinometer.

Although the wavelength selection for electron impact excitation is critical, there are a few exceptions, such as the oxygen atom's wavelength of 844.6 nm. Because dissociative excitation plays a significant role in producing oxygen atoms in plasma, certain studies used the 844.6 nm wavelength rather than the renowned 777 nm wavelength [29,30]. Selecting the wavelengths for molecules with actinometry is difficult. Electron impact excitation is important in the actinometry process, as aforementioned; many researchers have attempted to correlate the actinometry of molecules with their density, including N_2 , CO, CF, and CN [31–34]. Those researchers demonstrated similar connections although their wavelength did not match the electron impact excitation mechanism. We selected the CO, CN, N_2 , NO, O, and F peaks stated in Table 3 based on extensive investigation and discovered peaks noted in the previous paragraph, where CF, CF_2 , and N wavelengths were not selected because they were difficult to identify [30–37]. Figure 6a shows the obtained OES spectrum with N_2 gas flow rate variation, and Figure 6b shows the selected wavelengths from 8 sccm N_2 , which are N_2 FPS, SPS, N_2^+ FNS, fluorine at 704.1 and 686.5 nm, oxygen at 778.01 and 845.08 nm, CN at 338.92 nm, CO at 438.16, 297.73, and 283.27 nm, N_2 at 337.62, 381.1, and 394.79 nm, and NO at 247.42 and 259.07 nm. Table 3 lists the wavelengths that we could identify. Figure 7a–f shows the results of Ar actinometry with the wavelengths. Figure 7a,b shows that the number of fluorine atoms decreased, whereas the number of oxygen atoms remained almost constant. Kim et al. [38] discovered a comparable pattern in F concentration when N_2 was delivered more than a few sccms. Figure 7c shows that the reason why the concentration of O was maintained almost constant is that O atoms participated to form NO radicals, and the actinometry is unreliable because of the dissociative excitation. Figure 7d shows that the intensity of N_2 increased as its flow rate increased. CN in Figure 7e increased as the flow rate of N_2 increased, as in the case of NO and N_2 . Finally, Figure 7f shows that the trend for CO was either decreasing or nearly constant. Although this contradicts Premachandran's results, the N_2 concentration reported in that study was 1%, and the concentration of N_2 used in this study was affected by air leakage [39].

Table 3. Information on selected wavelengths used in actinometry.

Species	Shifted Wavelength (nm)	Transition	Threshold Energy (eV)
Ar	750.87	$3s^23p^5(^2P^{\circ}_{1/2})4p \rightarrow 3s^23p^5(^2P^{\circ}_{1/2})4s$	13.5
F	704.1	$2s^22p^4(^3P)3p \rightarrow 2s^22p^4(^3P)3s$	14.7
	686.5	$2s^22p^4(^3P)3p \rightarrow 2s^22p^4(^3P)3s$	14.5
O	845.08	$2s^22p^3(^4S^{\circ})3p \rightarrow 2s^22p^3(^4S^{\circ})3s$	11
	778.01	$2s^22p^3(^4S^{\circ})3p \rightarrow 2s^22p^3(^4S^{\circ})3s$	10.7
NO	259.07	$A^2\Sigma^+ \rightarrow X^2\Pi(0,3)$	–
	247.42	$A^2\Sigma^+ \rightarrow X^2\Pi(0,2)$	–
N_2	394.79	$C^3\Pi_u \rightarrow B^3\Pi_g(2,5)$	–
	381.1	$C^3\Pi_u \rightarrow B^3\Pi_g(0,2)$	–
	337.62	$C^3\Pi_u \rightarrow B^3\Pi_g(0,0)$	–
CN	388.92	$B^2\Sigma \rightarrow X^2\Sigma(0,0)$	–
CO	483.61	$B^1\Sigma \rightarrow A^1\Pi(0,1)$	–
	297.73	$b^3\Sigma^+ \rightarrow a^3\Pi(0,1)$	–
	283.27	$b^3\Sigma^+ \rightarrow a^3\Pi(0,0)$	–

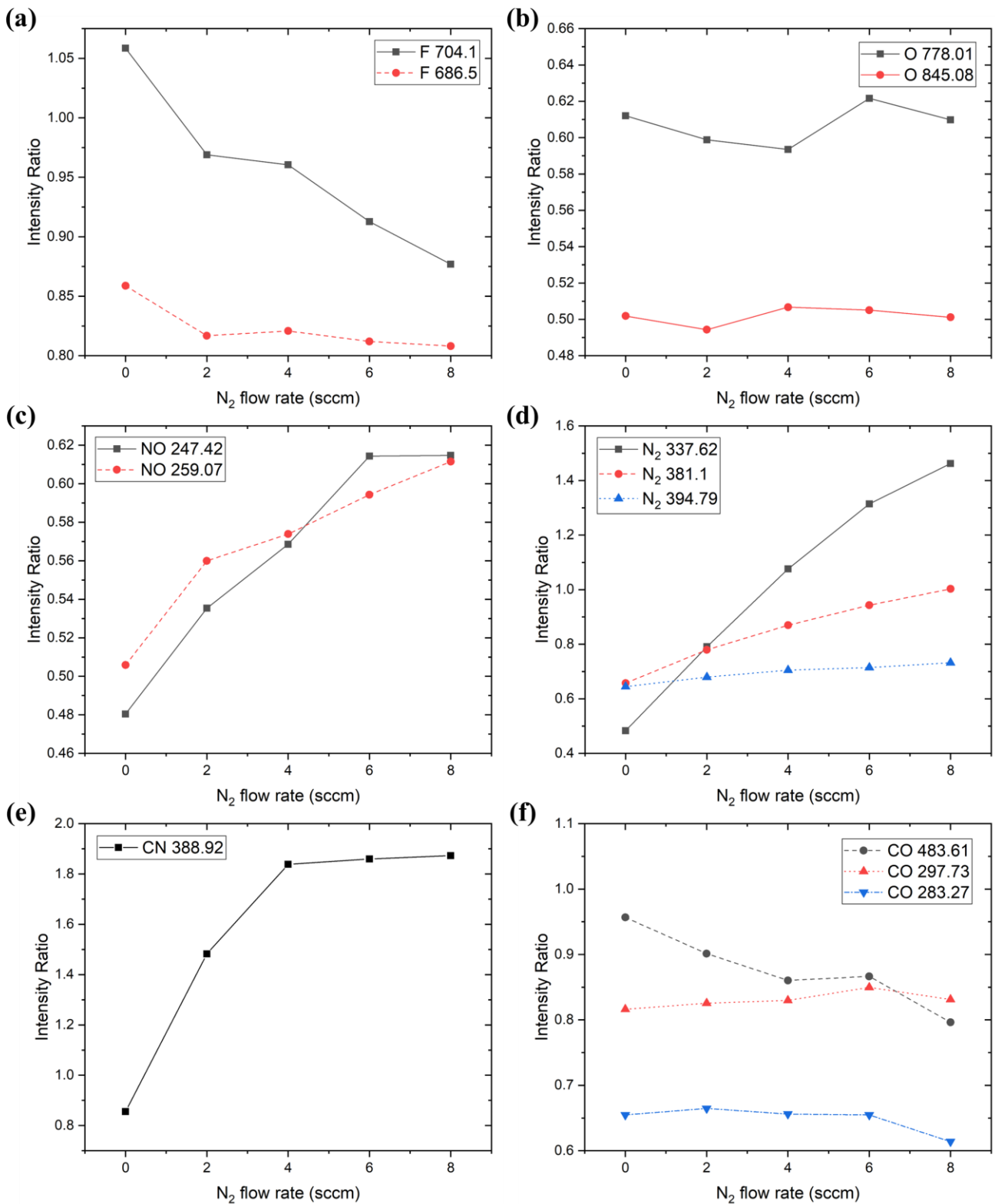


Figure 7. Actinometry results of (a) fluorine, (b) oxygen, (c) NO, (d) N₂, (e) CN, and (f) CO.

Si₃N₄ etching was performed under the same experimental conditions as N₂ flow rate split cases discussed in Figure 7 to assess the effect of the change in the number of radicals as the flow rate of N₂ increased. The Si₃N₄ etch rate was determined using a reflectometer to compare the thickness before and after etching. Figure 8 shows that the etch rate followed a similar pattern to the decreasing trend of F radicals owing to the measurement.

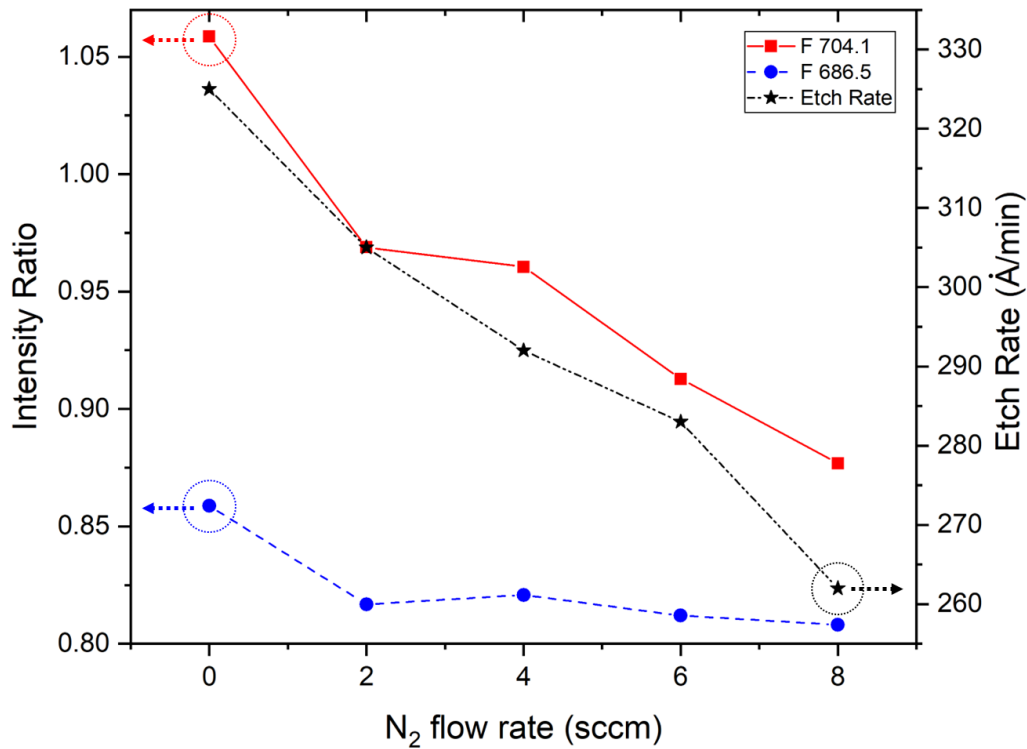


Figure 8. Trends of the F actinometry results versus the etch rate of Si₃N₄.

Furthermore, the cause for the F reduction and why the etch rate follows the same pattern as the F decrement was then explored. Notably, the number of F decreases in three primary situations: (1) reduction in the number of equations for the F generation, (2) increased F consumption, and (3) reduced F production. Chemkin was used to confirm the chemical reaction and determine which of the three factors had the most significant influence. When the number of equations to produce F was compared between the cases where only two species of CF₄ and O₂ were added and where three species added up to N₂ existed concurrently, it was confirmed that when N₂ was added, the number of equations for the formation of F increased, as shown in Table 4.

Table 4. The reaction of F production and consumption with and without N₂ addition.

		N ₂ Ejected	
Production	Consumption	Production	Consumption
CF ₄ + E => CF ₃ ⁺ + F + 2E	F + E => F ⁺ + 2E	CF ₄ + E => CF ₃ ⁺ + F + 2E	F + E => F ⁺ + 2E
CF ₄ + E => CF ₂ ⁺ + 2F + 2E	F + F ⁻ => F ₂ + E	CF ₄ + E => CF ₃ + F + E	F + F ⁻ => F ₂ + E
CF ₄ + E => CF ⁺ + F ₂ + F + 2E	F + O ₂ ⁻ => O ₂ + F ⁻	CF ₄ + E => 2F + CF ₂ + E	F + F ⁻ => 2F + E
CF ₄ + E => CF ₃ + F + E	F + CF ₃ => CF ₄	CF ₄ + E => F ₂ + CF + F + E	F + CF ₃ => CF ₄
CF ₄ + E => 2F + CF ₂ + E	F + CF ₂ => CF ₃	CF ₃ ⁺ + E => CF ₂ + F	F + CF ₂ => CF ₃
CF ₄ + E => F ₂ + CF + F + E	F + CF => CF ₂	CF ₃ + E => CF ₂ + F + E	F + COF => COF ₂
CF ₃ ⁺ + E => CF ₂ + F	F + COF => COF ₂	CF ₂ + E => CF + F + E	
CF ₃ + E => CF ₂ + F + E		CF ₂ + E => CF ⁺ + F + 2E	
CF ₃ + E => CF ₂ ⁺ + F + 2E		F ⁺ + E => F	
CF ₂ + E => CF + F + E		F ₂ + E => F + F ⁻	
CF ₂ + E => CF ⁺ + F + 2E		CF ₃ ⁺ + F ⁻ => 2F + CF ₂	
CF + E => C + F + E		CF ⁺ + F ⁻ => CF + F	
F ⁺ + E => F		F ₂ + F ⁻ => F + F ₂ + E	
F ₂ + E => F + F ⁻		F ⁺ + F ⁻ => 2F	
CF ₃ ⁺ + F ⁻ => 2F + CF ₂		CF ₃ ⁺ + F ⁻ => F + CF ₃	
CF ⁺ + F ⁻ => CF + F		F ⁺ + C => C ⁺ + F	
F + F ⁻ => 2F + E		CF ⁺ + F ⁻ => 2F + C	
F ₂ + F ⁻ => F + F ₂ + E		F ₂ + CF ₂ => CF ₃ + F	
F ⁺ + F ⁻ => 2F		F ₂ + CF ₃ => CF ₄ + F	
F ₃ ⁺ + F ⁻ => F + CF ₃		CF ⁺ + E => C + F	

Table 4. Cont.

		N ₂ Ejected	
Production	Consumption	Production	Consumption
F ⁺ + C => C ⁺ + F		O + F ⁻ => F + O + E	
CF ⁺ + F ⁻ => 2F + C		F ⁺ + O => O ⁺ + F	
F ₂ + CF ₂ => CF ₃ + F		FO + O => O ₂ + F	
F ₂ + CF ₃ => CF ₄ + F		O + CF ₂ => COF + F	
CF ⁺ + E => C + F		O + CF ₂ => 2F + CO	
O ₂ ⁺ + CF ₄ => CF ₃ ⁺ + O ₂ + F		O + CF ₃ => COF ₂ + F	
O + F ⁻ => F + O + E		O + COF => CO ₂ + F	
F ⁺ + O => O ⁺ + F		O* + CF ₃ => COF ₂ + F	
F ⁺ + O ₂ => O ₂ ⁺ + F		O* + CF ₂ => COF + F	
FO + O => O ₂ + F		O* + CF ₂ => 2F + CO	
O + CF => CO + F		O* + COF => CO ₂ + F	
O + CF ₂ => COF + F		O* + FO => O ₂ + F	
O + CF ₂ => 2F + CO		COF + E => CO + F + E	
O + CF ₃ => COF ₂ + F		C ⁺ + F ⁻ => F + C	
O + COF => CO ₂ + F		CF ₂ ⁺ + F ⁻ => F + CF ₂	
O* + CF => CO + F		O ₂ ⁺ + CF ₄ => CF ₃ ⁺ + O ₂ + F	
O* + CF ₃ => COF ₂ + F		F ⁺ + O ₂ => O ₂ ⁺ + F	
O* + CF ₂ => COF + F		CF ₃ + E => CF ₂ ⁺ + F + 2E	
O* + CF ₂ => 2F + CO			
O* + COF => CO ₂ + F			
O* + FO => O ₂ + F			
COF + E => CO + F + E			
CF + N => CN + F			
CF ₂ + N => 2F + CN			
CF ₃ + N => F ₂ + CN + F			
N ⁺ + F ⁻ => F + N			
N ₂ ⁺ + F ⁻ => F + N ₂			
C ⁺ + F ⁻ => F + C			
CF ₂ ⁺ + F ⁻ => F + CF ₂			

In Figure 9, there was a minor difference in F consumption, but it was not significant. Therefore, it was proven that the amount of F reduction itself had the most significant impact. Combining the earlier OES data with this simulation result showed that, immediately after N₂ was introduced, CF₄ did not decompose into F but changed into a different chemical, such as a compound bound to N.

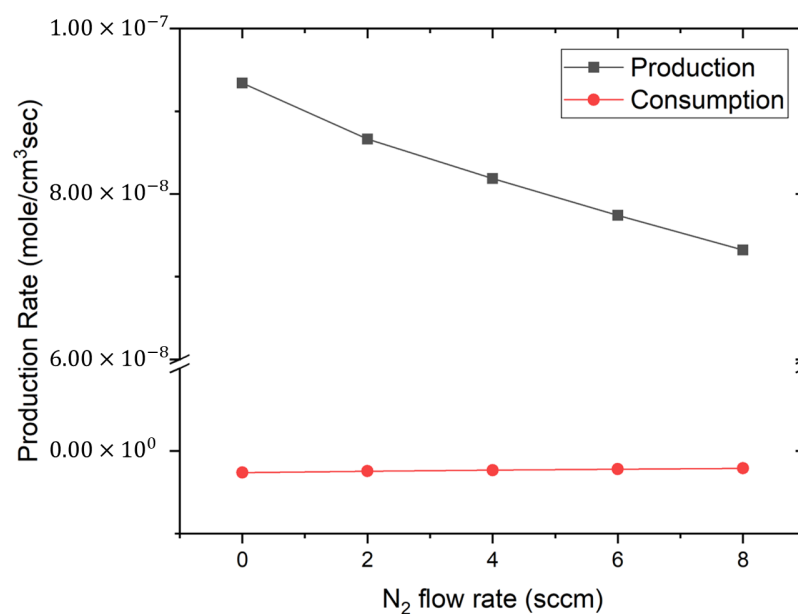


Figure 9. Production rate of the F atoms based on the N₂ flow rate. The consumption rate, shown in the red line, has a negative value since it uses the generated F atoms.

Table 5 describes the cause for the reduction in etch rate confirmed by the data thus far and the surface reaction mechanism. Si_3N_4 etching can be categorized into two parts as follows: Si atom and N atom etchings. First, in the Si atom etch mechanism, the surface is fluorinated by the F radicals created from the breakdown of CF_4 , and then four F atoms react with Si to form SiF_4 . Second, N atoms or NO molecules produced by the breakdown or combination of N_2 and $\text{N}_2 + \text{O}_2$ react with N atoms on the surface to evaporate as N_2 or N_2O in the N atom etch process. Therefore, it is possible to deduce that the reduction in the etch rate is due to the Si etch mechanism among Si_3N_4 becoming inactive due to the F decrease.

Table 5. Surface reaction mechanism in Si_3N_4 etching.

Reaction	Comment
$\text{F} + \text{SiN}(\text{s}) \rightarrow \text{SiNF}(\text{s})$	Fluorination
$\text{F} + \text{SiNF}(\text{s}) \rightarrow \text{SiNF}_2(\text{s})$	Fluorination
$\text{F} + \text{SiNF}_2(\text{s}) \rightarrow \text{SiNF}_3(\text{s})$	Fluorination
$\text{F} + \text{SiNF}_3(\text{s}) \rightarrow \text{SiF}_4 + \text{N}(\text{s})$	Fluorination and Desorption
$\text{NO} + \text{N}(\text{s}) \rightarrow \text{N}_2\text{O} + \text{SiN}(\text{s})$	Removal of Nitride Sites
$\text{N} + \text{N}(\text{s}) \rightarrow \text{N}_2 + \text{SiN}(\text{s})$	Removal of Nitride Sites
$\text{NO} + \text{N}(\text{s}) \rightarrow \text{N}_2 + \text{O}(\text{s})$	Oxidation of Nitride Sites
$\text{NO} + \text{O}(\text{s}) \rightarrow \text{NO}_2 + \text{SiN}(\text{s})$	Removal of Oxidized Sites
$\text{O} + \text{O}(\text{s}) \rightarrow \text{O}_2 + \text{SiN}(\text{s})$	Removal of Oxidized Sites
$\text{O}(\text{s}) + \text{O}(\text{s}) \rightarrow \text{O}_2 + \text{SiN}(\text{s})$	Removal of Oxidized Sites

4. Conclusions

In this study, the OES analysis method of CF_4/O_2 mixed with N_2 plasma and plasma reaction as a function of N_2 flow rate change was investigated. The OES data of individual gases and the mixed plasma of the two gases are first investigated because of the limitation that the OES wavelength shift and the emission wavelengths of numerous atoms, ions, and molecules in the mixed-gas plasma appear at nearly identical places. Then, radical species were defined in CF_4/O_2 mixed with N_2 plasma, which was our main goal. Additionally, the relative ratio of radicals was validated by actinometry using peaks previously identified as useful in prior investigations and previously selected peaks. F and CO decreased as the flow rate of N_2 increased, indicating that more compounds were binding to N. The production rate of F reduced as the flow rate of N_2 increased, which is the cause of the reduced quantity of F. Furthermore, the etch rate was reduced because F was required to etch Si in Si_3N_4 . We could successfully demonstrate how to analyze OES when CF_4/O_2 is mixed with N_2 and confirm the reaction based on the change in N_2 flow rate using these results. The effects of N_2 addition also revealed the Si_3N_4 etch and chemical simulation.

Author Contributions: Conceptualization, principal investigation, supervision, funding acquisition, writing—review and editing, S.J.H.; writing—review and editing, J.E.K.; methodology, validation, formal analysis, investigation, and data acquisition, W.S.S. All authors have read and agreed to the published version of the manuscript.

Funding: This work was supported by the National Research Council of Science and Technology under the Plasma E. I. (Grant ID: 1711121944, CRC-20-01-NFRI) and Korea Institute for Advancement of Technology (KIAT) grant funded by Korea Government (MOTIE). (P0008458, The Competency Development Program for Industry Specialist).

Institutional Review Board Statement: Not applicable.

Informed Consent Statement: Not applicable.

Data Availability Statement: Data will be made available upon request.

Acknowledgments: Authors are grateful to Lee at Korea Spectral Products for assisting with the SM245 spectrometer and the Semiconductor Process Diagnosis Research Center (SPDRC) at Myongji University for their skillful 300 mm fab equipment and facility.

Conflicts of Interest: The authors declare no conflict of interest.

References

1. Arienzo, M.; Orr-Arienzo, W.A. Silicon Nitride in Semiconductor Device Technology. In *Materials Science Forum*; Trans Tech Publication, Ltd.: Bäch, Switzerland, 1991; Volume 47, pp. 228–248. [\[CrossRef\]](#)
2. Kim, B.; Hong, S.J. In-Situ Virtual Metrology for the Silicon-Dioxide Etch Rate by using Optical Emission Spectroscopy Data. *J. Korean Phys. Soc.* **2014**, *65*, 168–175. [\[CrossRef\]](#)
3. Cheng, Y.; Lee, C.; Haung, C. Plasma Damage on Low-k Dielectric Materials. In *Plasma Science and Technology-Basic Fundamentals and Modern Applications*; IntechOpen: Vienna, Austria, 2018; Volume 15, pp. 291–318. [\[CrossRef\]](#)
4. King, S.W.; French, M.; Bielefeld, J.; Lanford, W.A. Fourier Transform Infrared Spectroscopy Investigation of Chemical Bonding in Low-k a-SiC: H Thin Films. *J. Non-Cryst. Solids* **2011**, *357*, 2970–2983. [\[CrossRef\]](#)
5. Wallace, R.M. In-Situ Studies of Interfacial Bonding of High-k Dielectrics for CMOS Beyond 22 nm. *ECS Trans.* **2008**, *16*, 255–271. [\[CrossRef\]](#)
6. Cleveland, E.R.; Ruppalt, L.B.; Bennett, B.R.; Prokes, S.M. Effect of an In Situ Hydrogen Plasma Pre-Treatment on the Reduction of GaSb Native Oxides Prior to Atomic Layer Deposition. *Appl. Surf. Sci.* **2013**, *277*, 167–175. [\[CrossRef\]](#)
7. Jang, J.; Kim, H.-S.; Cho, W.; Cho, H.; Kim, J.; Shim, S.I.; Jang, Y.; Jeong, J.-H.; Son, B.-K.; Kim, D.W.; et al. Vertical Cell Array Using TCAT (Terabit Cell Array Transistor) Technology for Ultra High Density NAND Flash Memory. In Proceedings of the Symposium on VLSI Technology, Kyoto, Japan, 15–17 June 2009.
8. Choi, J.E.; Song, J.; Lee, Y.H.; Hong, S.J. Deep Neural Network Modeling of Multiple Oxide/Nitride Deposited Dielectric Films for 3D-NAND Flash. *Appl. Sci. Converg. Technol.* **2020**, *29*, 190–194. [\[CrossRef\]](#)
9. Khan, A.H.; Srinivasan, S.; Choi, J.; Athayde, A.; Achutharaman, R. Etch Challenges for 3D NAND Flash Technology. In Proceedings of the ECS and SMEQ Joint International Meeting, Cancun, Mexico, 5–9 October 2014. [\[CrossRef\]](#)
10. Clarke, P.E.; Field, D.; Hydes, A.J.; Klemperer, D.F.; Seakins, M.J. Mass Spectrometric Studies of Plasma Etching of Silicon Nitride. *J. Vac. Sci. Technol. B Microelectron. Nanometer Struct.* **1985**, *3*, 1614. [\[CrossRef\]](#)
11. Field, D.; Klemperer, D.F.; Wade, I.T. Spectroscopic Studies of Fluorescent Emission in Plasma Etching of Silicon Nitride. *J. Vac. Sci. Technol. B Microelectron. Process. Phenom.* **1988**, *6*, 551. [\[CrossRef\]](#)
12. Reyes-Betanzo, C.; Moshkalyov, S.A.; Swart, J.W.; Ramos, A. Silicon Nitride Etching in High- and Low-Density Plasmas using SF₆/O₂/N₂ Mixtures. *J. Vac. Sci. Technol. A Vac. Surf. Film* **2003**, *21*, 461. [\[CrossRef\]](#)
13. Barsukov, Y.; Volynets, V.; Lee, S.; Kim, G.; Lee, B.; Nam, S.K.; Han, K. Role of NO in Highly Selective SiN/SiO₂ and SiN/Si Etching with NF₃/O₂ Remote Plasma: Experiment and Simulation. *J. Vac. Sci. Technol. A Vac. Surf. Film* **2017**, *35*, 061310. [\[CrossRef\]](#)
14. Huang, S.; Volynets, V.; Hamilton, J.R.; Nam, S.K.; Song, I.; Lu, S.; Tennyson, J.; Kushner, M.J. Downstream Etching of Silicon Nitride using Continuous-Wave and Pulsed Remote Plasma Sources Sustained in Ar/NF₃/O₂ Mixtures. *J. Vac. Sci. Technol. A Vac. Surf. Film* **2018**, *36*, 021305. [\[CrossRef\]](#)
15. Kuboi, N.; Tatsumi, T.; Kinoshita, T.; Shigetoshi, T.; Fukasawa, M.; Komachi, J.; Ansai, H. Prediction of Plasma-Induced Damage Distribution during Silicon Nitride Etching using Advanced Three-Dimensional Voxel Model. *J. Vac. Sci. Technol. A Vac. Surf. Film* **2015**, *33*, 061308. [\[CrossRef\]](#)
16. Prévost, E.; Cunge, G.; De-Buttet, C.; Lagrasta, S.; Vallier, L.; Petit-Etienne, C. Study of selective chemical downstream plasma etching of silicon nitride and silicon oxide for advanced patterning applications. In Proceedings of the SPIE Advanced Lithography, San Jose, CA, USA, 26 February–2 March 2017. [\[CrossRef\]](#)
17. Shinoda, K.; Miyoshi, N.; Kobayashi, H.; Izawa, M.; Saeki, T.; Ishikawa, K.; Hori, M. Self-Limiting Reactions of Ammonium Salt in CHF₃/O₂ Downstream Plasma for Thermal-Cyclic Atomic Layer Etching of Silicon Nitride. *J. Vac. Sci. Technol. A Vac. Surf. Film* **2019**, *37*, 051002. [\[CrossRef\]](#)
18. Hsiao, S.N.; Nguyen, T.-T.-N.; Tsutsumi, T.; Ishikawa, K.; Sekine, M.; Hori, M. Etching Characteristics of PECVD-Prepared SiN Films with CF₄/D₂ and CF₄/H₂ Plasmas at Different Temperatures. In Proceedings of the 2020 International Symposium on Semiconductor Manufacturing (ISSM), Tokyo, Japan, 15–16 December 2020. [\[CrossRef\]](#)
19. Hamada, T.; Masuda, S.; Nishida, K.; Yamamoto, S. Etching Characteristics of Si_xN_y Film on Textured Single Crystalline Silicon Surface using Ar/CF₄ and He/CF₄ Surface-Discharge Plasma. *Coatings* **2020**, *10*, 563. [\[CrossRef\]](#)
20. Jang, D.B.; Hong, S.J. In-Situ Monitoring of Multiple Oxide/Nitride Dielectric Stack PECVD Deposition Process. *Trans. Electr. Electron. Mater.* **2018**, *19*, 21–26. [\[CrossRef\]](#)
21. Jang, Y.; Roh, H.; Park, S.; Jeong, S.; Ryu, S.; Kwon, J.; Kim, N.; Kim, G. Characteristics of a Plasma Information Variable in Phenomenology-Based, Statistically-Tuned Virtual Metrology to Predict Silicon Dioxide Etching Depth. *Curr. Appl. Phys.* **2019**, *19*, 1068–1075. [\[CrossRef\]](#)
22. Rachdi, L.; Hofmann, M. Use of Optical Emission Spectroscopy to Predict Silicon Nitride Layer Properties. *Vacuum* **2021**, *191*, 110322. [\[CrossRef\]](#)
23. Zhu, X.; Pu, Y. Optical Emission Spectroscopy in Low-Temperature Plasmas Containing Argon and Nitrogen: Determination of the Electron Temperature and Density by the Line-Ratio Method. *J. Phys. D* **2010**, *43*, 403001. [\[CrossRef\]](#)

24. Evdokimov, K.E.; Konishev, M.E.; Pichugin, V.F.; Sun, Z. Study of Argon Ions Density and Electron Temperature and Density in Magnetron Plasma by Optical Emission Spectroscopy and Collisional-Radiative Model. *Res. Eff. Technol.* **2017**, *3*, 187–193. [[CrossRef](#)]
25. Onishi, H.; Yamazaki, F.; Hakozaki, Y.; Takemura, M.; Nezu, A.; Akatsuka, H. Measurement of Electron Temperature and Density of Atmospheric-Pressure Non-Equilibrium Argon Plasma Examined with Optical Emission Spectroscopy. *Jpn. J. Appl. Phys.* **2021**, *60*, 026002. [[CrossRef](#)]
26. Chien, K.; Chang, C.; Djurdjanovic, D. Virtual Metrology Modeling of Reactive Ion Etching Based on Statistics-Based and Dynamics-Inspired Spectral Features. *J. Vac. Sci. Technol. B Nanotechnol. Microelectron. Mater. Process. Meas. Phenom.* **2021**, *39*, 064003. [[CrossRef](#)]
27. Kim, W.J.; Bang, I.Y.; Kim, J.H.; Park, Y.S.; Kwon, H.T.; Shin, G.W.; Kang, M.; Cho, Y.; Kwon, B.; Kwak, J.H. Etching Characteristics of NF_3 and F_3NO at Reactive Ion Etching Plasma for Silicon Oxide and Silicon Nitride. *J. Korean Phys. Soc.* **2021**, *79*, 290–296. [[CrossRef](#)]
28. Xu, D.; Zou, S.; Xin, Y.; Su, X.; Wang, X. Characteristics of Dual-Frequency Capacitively Coupled SF_6/O_2 Plasma and Plasma Texturing of Multi-Crystalline Silicon. *Chin. Phys. B* **2014**, *23*, 065201. [[CrossRef](#)]
29. Duluard, C.Y.; Dussart, R.; Tillocher, T.; Pichon, L.E.; Lefauchaux, P.; Puech, M.; Ranson, P. SO_2 Passivating Chemistry for Silicon Cryogenic Deep Etching. *Plasma Sources Sci. Technol.* **2008**, *17*, 045008. [[CrossRef](#)]
30. Cruden, B.A.; Rao, M.; Sharma, S.P.; Meyyappan, M. Fourier-Transform Infrared and Optical Emission Spectroscopy of $\text{CF}_4/\text{O}_2/\text{Ar}$ Mixtures in an Inductively Coupled Plasma. *J. Appl. Phys.* **2003**, *93*, 5053–5062. [[CrossRef](#)]
31. Czerwicz, T.; Greer, F.; Graves, D.B. Nitrogen Dissociation in a Low Pressure Cylindrical ICP Discharge Studied by Actinometry and Mass Spectrometry. *J. Phys. D* **2005**, *38*, 4278. [[CrossRef](#)]
32. Kawata, H.; Takao, Y.; Murata, K.; Nagami, K. Optical Emission Spectroscopy of CF_4+O_2 Plasmas using a New Technique. *Plasma Chem. Plasma Process.* **1988**, *8*, 189–206. [[CrossRef](#)]
33. Kiss, L.; Nicolai, J.; Conner, W.T.; Sawin, H.H. CF and CF_2 Actinometry in a CF_4/Ar Plasma. *J. Appl. Phys.* **1992**, *71*, 3186–3192. [[CrossRef](#)]
34. Jamroz, P.; Zyrnicki, W. Optical Emission Characteristics of Glow Discharge in the $\text{N}_2\text{-H}_2\text{-Sn}(\text{CH}_3)_4$ and $\text{N}_2\text{-Ar-Sn}(\text{CH}_3)_4$ Mixtures. *Surf. Coat. Technol.* **2006**, *201*, 1444–1453. [[CrossRef](#)]
35. Kimura, T.; Hanaki, K. Experiments and Global Model Analysis of Inductively Coupled $\text{CF}_4/\text{O}_2/\text{Ar}$ Plasmas. *Jpn. J. Appl. Phys.* **2008**, *47*, 8537. [[CrossRef](#)]
36. Li, J.; Kim, S.J.; Han, S.; Kim, Y.; Chae, H. Etching Characteristics of Hydrogenated Amorphous Carbon with Different sp^2/sp^3 Hybridization Ratios in CF_4/O_2 Plasmas. *Plasma Process. Polym.* **2021**, *18*, 2100075. [[CrossRef](#)]
37. Ichikawa, Y.; Sakamoto, T.; Nezu, A.; Matsuura, H.; Akatsuka, H. Actinometry Measurement of Dissociation Degrees of Nitrogen and Oxygen in $\text{N}_2\text{-O}_2$ Microwave Discharge Plasma. *Jpn. J. Appl. Phys.* **2010**, *49*, 106101. [[CrossRef](#)]
38. Kim, Y.S.; Jeon, S.H.; Jung, C.H. Fluorination Reaction of Uranium Dioxide in $\text{CF}_4/\text{O}_2/\text{N}_2$ Rf Plasma. *Ann. Nucl. Energy* **2003**, *30*, 1199–1209. [[CrossRef](#)]
39. Premachandran, V. Enhanced Etching of Silicon in $\text{CF}_4\text{-O}_2\text{-N}_2$ Plasma. *Appl. Phys. Lett.* **1990**, *57*, 678–679. [[CrossRef](#)]